A Cascading Approach for Multi-frequency Widelanes and Extra-Widelanes Carrier Phase Integer Ambiguity Resolution

Clément Gazzino, Nicolas Lelarge, *Centre National d'Études Spatiales, Toulouse, France*

BIOGRAPHY

Clément Gazzino graduated from the French High Institute for Aeronautics and Space and obtained his master of engineering with a space systems specialisation. He obtained his PhD degree in space trajectory optimisation from the university of Toulouse. He is now working at the navigation department at CNES, the French space agency, and he is involved in the development of precise point positioning algorithms.

Nicolas Lelarge graduated from the French High Institute for Aeronautics and Space and obtained his master of engineering with a space systems specialisation. He is a member of the navigation system department at CNES, the French space agency, and he is involved in the development of precise point positioning algorithms.

ABSTRACT

Precise Point Positioning (PPP) in Global Navigation Satellite Systems (GNSS) relies on the resolution of carrier phase ambiguities to achieve high-precision positioning. Usualy, ambiguity resolution has relied on widelane or Melbourne-Wübbena combinations of two frequencies. However, with the development of new generation satellite constellations and the advent of multi-frequency GNSS signals, the potential for utilizing more than two signals in ambiguity resolution has emerged. Studies have explored this potential using various systems such as GPS, Beidou, and Galileo, which employ up to four frequencies. Despite their benefits, ionosphere-free integer phase combinations often suffer from large noise amplification factors or result in small wavelengths. Conversely, traditional widelane combinations, while maintaining a reasonable noise amplification factor, tend to amplify ionospheric delays, which can be difficult to estimate with the necessary precision. In this paper, we propose a novel method that optimizes the use of code, carrier-phase and Doppler measurement at multiple frequencies to enhance ambiguity resolution in PPP. Our approach mitigates the limitations of existing combinations by balancing noise amplification and ionospheric delay effects; and allows instantaneous extra-widelanes fixation, and very fast widelanes fixations.

Keywords: Precise Point Positioning, GNSS, Ambiguity resolution, Multi-frequency, Widelane combination, Ionosphere-free combination

I Introduction

Centimeter range positioning accuracy with the use of the Global Navigation Satellite Systems (GNSS) can be achieved by the processing of the carrier-phase (phase) of the transmitted signal, together with the pseudo-range (code) and the Doppler shift measurements – see (Kaplan and Hegarty, 2006, Chapter 8) and the reference therein – with the assumption that all the error sources are unbiased and the phase ambiguity is properly estimated. This opened the door for the Real-Time Kinematic (RTK) and the Precise Point Positioning (PPP) techniques for high-precision positioning (Groves, 2008, Chapter 8). The determination of the integer ambiguity is an essential process to grant high precision GNSS estimation. A prerequisite for integer ambiguity resolution (IAR) on the receiver side is the need of a ground station network for computing the precise satellite orbits and clocks as well as the satellite code and phase biases. The French Centre National d'Études Spatiales (CNES) has set up such a station network and a demonstrator Laurichesse (2011) based on the undifferenced satellite phase bias estimation described in Laurichesse (2012) and Laurichesse and Privat (2015) that allows to compute and disseminate undifferenced Observable Specific Biases (OSB) in the Radio Technical Commission for Maritime Service (RTCM) or the State Space Representation (SSR) format.

Once the satellite precise orbits, clocks, code, and phase biases are retrieved by the receiver, the phase integer ambiguities have to be solved, and the corresponding biases have to be identified in order to enable very accurate PPP solutions. Recent PPP algorithms take advantage of the third and fourth frequency of the GPS, Galileo, and Beidou constellations, see for instance Liu et al. (2021). In particular, the reference Laurichesse and Banville (2018) has demonstrated that fast convergence using the Galileo third frequency can be achieved, and has been added to the CNES user software for PPP presented in Laurichesse and Privat (2015).

Previous studies have attempted to take advantage of the frequencies available from GPS, Beidou and Galileo – Cocard et al. (2008), Li et al. (2020), and Ji et al. (2022) respectively – to help fixing the ambiguities. Despite their benefits, the new ionosphere-free integer phase combinations introduced suffer from large noise amplification factors or result in small wavelengths, preventing

the user from efficiently fixing the integer ambiguities.

The objective of this paper is to develop a new approach for instantaneously estimating the extra-widelane (EWL) phase ambiguity without any convergence phase. A Kalman filter is commonly used to solve the positioning problem. Our method employs a new cascading scheme to take advantage of the previously fixed EWL to help in fixing the subsequent widelane (WL). The integer constraints are applied with a bootstrap method, as described in (Teunissen and Montenbruck, 2017, Chapter 20), after the update step of the Kalman filter. Taking into account all ambiguities in the filter leads to a high-dimensional state vector. The proposed approach thus aims at reducing the complexity of the estimation problem. The second step of the proposed method thus focuses on a reduced-size Kalman filter for the estimation of the WL ambiguity, following the EWL – WL ambiguity decomposition introduced in Zhao et al. (2022) and Gazzino et al. (2023). This method is applied to increase the WL integer ambiguity fixation ratio for measures gathered from a ground station and a dynamical run.

II Fixing the Extra-Widelanes ambiguities instantaneously

1 GNSS measurements modeling

The pseudorange (code), carrier-phase (phase) and Doppler measurements from a GNSS satellite s at the frequency f_i (and wavelength λ_i) observed by a receiver r are modeled as:

$$\begin{aligned} C_i &= \rho_r^s + h_r^s + \gamma_i e^s + m(E^s)T_z + b_{r,C_i}^s, \\ \lambda_i L_i &= \rho_r^s + h_r^s - \gamma_i e^s + m(E^s)T_z + \lambda_i N_{r,i}^s + b_{r,L_i}^s, \\ D_i &= -\lambda_i \Delta f_i = \dot{\rho}_r^s + \dot{h}_r^s - \gamma_i \dot{e}^s, \end{aligned} \tag{1}$$

where C_i is the code measurement expressed in the unit of distance, L_i is the phase measurement expressed in the unit of cycles at the frequency $f_i = c/\lambda_i$ with c the speed of light in vacuum, and D_i is the equivalent Doppler shift measurement expressed in the unit of distance per time. The quantities $h_r^s = h_r - h^s$ is the clock offset between the satellite and the receiver, e^s is the slant ionospheric delay at the reference frequency $f_1 = 1575.42$ MHz (corresponding to the L1 / E1 signals) for the satellite s, $\gamma_i = f_1^2/f_i^2$, T_z is the zenithal wet tropospheric delay, $m(E^s)$ is the mapping function depending on the satellite elevation E^s of the satellite s, and $N_{r,i}^s$ is the phase ambiguity of the signal coming from the satellite s at the frequency f_i. The difference between the code and phase sofware and hardware biases at the satellite and receiver levels on the frequency f_i is denoted, respectively, as $b_{r,C_i}^s = b_{r,C_i} - b_{C_i}^s$ and $b_{r,L_i}^s = b_{r,L_i} - b_{L_i}^s$. ρ_r^s is the geometric distance between the satellite s and the receiver r including the phase center offset correction.

The Doppler shift measurement Δf_i is the difference between the observed and emitted frequency of the carrier; its sign is usually defined positive for approaching satellites. For convenience, we will denote $\bar{L}_i = L_i - N_i^s$ the unambiguous phase measurement. To make the equations simpler, phenomena like the wind-up effect, Shapiro effect, Sagnac effect, phase center offset and zenithal dry tropospheric delay were removed from the measurements and supposed to be already taken into account.

The undifferenced satellite code and phase biases, as well as the satellite part of the clock offset, are retrieved from existing products. In our case they are retrieve from the ones computed by the PPP-WIZARD demonstrator as described in the reference Laurichesse (2011). The code and phase equations are thus modified to remove the already known components from the right-hand side. With this definition, the code and phase measurement models at the frequency f_j are rewritten as:

$$\begin{aligned} \tilde{C}_j &= C_j + h^s + b_{C_j}^s = \rho_r^s + h_r + b_{r,C_j} + \gamma_j e^s + m(E^s)T_z \\ \lambda_j \tilde{L}_j &= \lambda_j L_j + h^s + b_{L_j}^s - \lambda_j W = \rho_r^s + h_r + b_{r,L_j} - \gamma_j e^s + m(E^s)T_z + \lambda_j N_{r,j}^s \\ \tilde{D}_j &= D_j + \dot{h}_s = \dot{\rho}_r^s + \dot{h}_r - \gamma_i \dot{e}^s, \end{aligned} \tag{2}$$

the multipath delay is not taken into account in this model, and lies in the observation noise. For readability reasons, the tilda superscript of the receiver observables will be removed throughout the remainder of the article.

The WL combinations are used to create a signal with a significantly large wavelength. This longer wavelength is useful for cycle-slips detection and ambiguity fixing. The WL combination of the phase measurements at the frequencies f_i and f_j is expressed in cycles by:

$$L_{\text{WL},ij} = L_i - L_j = \left(\frac{1}{\lambda_i} - \frac{1}{\lambda_j}\right)\left(\rho_r^s + h_r + m(E^s)T_z\right) - \left(\frac{\gamma_i}{\lambda_i} - \frac{\gamma_j}{\lambda_j}\right)e^s + N_{r,\text{WL},ij}^s + b_{r,\text{WL},ij}, \tag{3}$$

with $N_{\text{WL},ij}^s = N_i^s - N_j^s$ the WL ambiguity and $b_{r,\text{WL},ij}$ the WL receiver bias. In the subsequent sections, the geometrical part of the phase WL measure will be denoted as $D_r^s = \rho_r^s + h_r + m(E^s)T_z$, and the following geometric and ionospheric coefficients are defined:

$$\delta_{ij} = \frac{1}{\lambda_i} - \frac{1}{\lambda_j}, \quad \epsilon_{ij} = \frac{\gamma_i}{\lambda_i} - \frac{\gamma_j}{\lambda_j}. \tag{4}$$

If both f_i and f_j are close, the WL combination may be called EWL due to its very long wavelength. The noise of the combination is computed from Equation (3) assuming that the emitted signals are not correlated. The computed values, as well as the WL wavelength are displayed in the Table 1. The WL combinations $L_{\text{WL},5a5b}$, $L_{\text{WL},5a6}$ and $L_{\text{WL},5b6}$ are the EWL combinations. It has to be notted that building the WL combinations leads to an inflation of the ionospheric slant delay.

The standard deviations for the code and phase noise have been assumed to be 0.5 m and 0.003 m, respectively. These values will be employed throughout this article for the theoretical noise analysis.

Combination $L_{\text{WL},ij}$	$L_{\text{WL},5a5b}$	$L_{\text{WL},5a6}$	$L_{\text{WL},5b6}$	$L_{\text{WL},5a1}$	$L_{\text{WL},5b1}$	$L_{\text{WL},61}$
$\lambda_{\text{WL},ij}$ [m]	9.768	2.931	4.186	0.751	0.814	1.011
$\sigma_{L_{\text{WL},ij}}$ [m]	0.165	0.051	0.074	0.015	0.016	0.021
$\sigma_{L_{\text{WL},ij}}$ [0.01 cy]	1.687	1.739	1.760	1.968	1.986	2.030

Table 1: Wavelength and noise standard deviation of the Galileo WL and EWL.

2 Ambiguity fixing with the Melbourne-Wübbena combination

It has been shown in Laurichesse and Langley (2015), and verified later in Zhao et al. (2022), that it is preferable to build the phase WL and EWL combinations with their respective ambiguities rather than estimating the full system of the code and phase measurements on each frequency taken separately. To this end, it is necessary to build the Melbourne-Wübbena (MW) combination – see Melbourne (1985); Wübbena (1985) – $L_{\text{MW},ij}$, as a linear combination of the phase WL $L_{\text{WL},ij}$ and the code narrowlane (NL) $C_{\text{NL},ij}$:

$$L_{\text{MW},ij} = L_{\text{WL},ij} - C_{\text{NL},ij} = L_i - L_j + \frac{\lambda_i - \lambda_j}{\lambda_i + \lambda_j}\left(\frac{C_i}{\lambda_i} + \frac{C_j}{\lambda_j}\right) = N^s_{r,\text{WL},ij} + b_{r,\text{MW},ij} \tag{5}$$

with $b_{\text{MW},ij}$ the MW receiver bias.

The noise level of such a combination is computed from Equation (5) assuming that the observables are not correlated between them and is displayed in the Table 2.

$L_{\text{MW},ij}$	$L_{\text{MW},5a5b}$	$L_{\text{MW},5a6}$	$L_{\text{MW},5b6}$	$L_{\text{MW},5a1}$	$L_{\text{MW},5b1}$	$L_{\text{MW},61}$
$\lambda_{\text{WL},ij}$ [m]	9.768	2.931	4.186	0.751	0.814	1.011
$\sigma_{\Phi_{\text{MW},ij}}$ [m]	0.390	0.358	0.361	0.358	0.357	0.356
$\sigma_{L_{\text{MW},ij}}$ [0.01 cy]	3.993	12.200	8.630	47.584	43.856	35.234

Table 2: Table of wavelength and standard deviations in meters and cycles for the different Melbourne-Wübbena combinations for Galileo.

The carrier-to-noise level of the MW combinations of the three EWL combinations L_{5a5b}, L_{65a} and L_{65b} is of the order of magnitude of a tens of a cycle, or even below. Although the MW combination is often used for phase cycle slips detection (see for instance Bezmenov et al. (2019) and the references therein), such a low carrier-to-noise ratio paves the way for a direct estimation of the EWL ambiguity at each epoch without any filter convergence effect.

Assuming that n_S satellites are in view of the receiver at a given epoch, an observation model can be built to link the WL measures, the unknown phase ambiguities, and the receiver bias as:

$$\forall s \in \{1, \ldots, n_S\},\ L^s_{\text{MW},ij} = N^s_{r,\text{WL},ij} + b_{r,\text{MW},ij}. \tag{6}$$

The receiver MW bias is chosen to maximize the number of floating ambiguities approaching an integer value. The optimal bias value m^* is computed according to Algorithm 1. This algorithm takes as input the list of visible satellites as well as an ambiguity threshold α_N allowing to decide if a floating ambiguity is close enough to the nearest integer. The $\lfloor \cdot \rfloor$ operator stands for the integer part of a floating point number. The algorithm is run epoch by epoch, with the α_N parameter arbitrarily chosen to be 0.15 cycles.

Algorithm 1 Instantaneous EWL ambiguity fixing algorithm.

Require: $\mathbf{m}$ a list of test biases
Require: $\mathbf{s}$ the list of visible satellites
Require: α_N the ambiguity threshold parameter
  for $m \in \mathbf{m}$ **do**
    for $s \in \mathbf{s}$ **do**
      build the set $S(m) = \left\{ s \text{ such that } \left| L^s_{\text{MW},ij} - \lfloor L^s_{\text{MW},ij} \rfloor + m \right| \leqslant \alpha_N \right\}$
      compute $N(m)$ the cardinal of the set $S(m)$
    end for
  end for
  Choose $m^* = \text{argmax} N(m)$

It has to be noted that the WL ambiguity $N^s_{\text{WL},ij}$ depends on the satellite, whereas the bias receiver $b_{r,\text{MW},ij}$ depends on the receiver and thus remains constant across all the visible satellites. However, due to the rank deficiency of the system (6), the biases and all the ambiguities can shift in the opposite direction by the same integer value. Let n be an arbitrary integer number, and the new ambiguities defined as:

$$\forall s \in \{1, \ldots, n_S\},\ \tilde{N}^s_{r,\text{WL},ij} = N^s_{r,\text{WL},ij} + n. \tag{7}$$

With this transformation, the Equation (6) still holds if a new receiver bias $\tilde{b}_{r,\text{MW},ij}$ is defined by shifting the original one by the integer value $-n$:

$$\forall s \in \{1, \ldots, n_S\},\ L^s_{\text{WL},ij} = N^s_{r,\text{WL},ij} + b_{r,\text{MW},ij} = \left(N^s_{r,\text{WL},ij} + n\right) + \left(b_{r,\text{MW},ij} - n\right) = \tilde{N}^s_{r,\text{WL},ij} + \tilde{b}_{r,\text{MW},ij} \tag{8}$$

To address this issue and prevent any unwanted and artificial integer jumps after having performed the ambiguity fixing procedure, a new technique is proposed. Instead of detecting the phase cycle slips on the MW combination, the detection is performed on the estimated MW receiver bias. The cycle-slips detector used is the one described in Subirana et al. (2013). An empirical mean and standard deviations are estimated, and a jump is detected if the actual bias value is too far from the predicted one.

3 The cascading approach

The MW combinations built from the EWL have a carrier-to-noise ratio far less than a quarter of a cycle (see Table 2), and the integer ambiguities can thus be easily distinguished from the receiver bias. It follows that the $N^s_{r,\text{WL},5b5a}$, $N^s_{r,\text{WL},65a}$ and $N^s_{r,\text{WL},65b}$ ambiguities can be instantaneously fixed with a high success rate. The easiest ambiguity to fix is $N^s_{r,\text{WL},5b5a}$. Instead of fixing $N^s_{r,\text{WL},65a}$ and $N^s_{r,\text{WL},65b}$ independently, the key idea behind the cascading approach is to benefit from the already obtained unambiguous $L_{\text{WL},5b5a}$ to determine the other EWL ambiguities.

To this end, we consider a WL combination $L_{\text{WL},kl}$ whose ambiguity $N^s_{r,\text{WL},kl}$ has to be fixed, the WL combination $\bar{L}_{\text{WL},ij}$ whose ambiguity $N^s_{r,\text{WL},ij}$ has already been fixed to an integer thanks to the Algorithm 1 applied on the Melbourne-Wübbena combination $L_{\text{MW},ij}$, and a code measurement C_m at the frequency f_m. For the code measurement, the following notation will be considered: $\delta_m = \lambda_m^{-1}$, and $\varepsilon_m = \lambda_m^{-1}\gamma_m$. We are interested in finding the coefficients of the combination such that the geometry and the ionosphere parts vanish. The ionosphere-free geometry-free combinations $\mathcal{L}_{kl,ij,m}$ of the $L_{\text{WL},kl}$ and $\bar{L}_{\text{WL},ij}$ WL together with the code measurement C_m is given by:

$$\begin{aligned}
\mathcal{L}_{kl,ij,m} &= L^s_{\text{WL},kl} + \alpha \bar{L}^s_{\text{WL},ij} + \beta\delta_m C^s_m, \\
&= \left(\delta_{kl} D^s_r - \varepsilon_{kl} e^s + b_{r,\text{WL},kl} + N^s_{r,kl}\right) + \alpha\left(\delta_{ij} D^s_r - \varepsilon_{ij} e^s + b_{r,\text{WL},ij}\right) + \beta\delta_m\left(D^s_r + \gamma_m e^s + b_{r,C_m}\right) \\
&= \left(\delta_{kl} + \alpha\delta_{ij} + \beta\delta_m\right) D^s_r + \left(-\varepsilon_{kl} - \alpha\varepsilon_{ij} + \beta\varepsilon_m\right) e^s + \left(b_{r,\text{WL},kl} + \alpha b_{r,\text{WL},ij} + \beta\delta_m b_{r,C_m}\right) + N^s_{r,kl}
\end{aligned} \tag{9}$$

In order to cancel the ionospheric and the geometric term, the following conditions have to be fulfilled:

$$\delta_{kl} + \alpha\delta_{ij} + \beta\delta_m = 0 \quad \text{and} \quad -\varepsilon_{kl} - \alpha\varepsilon_{ij} + \beta\varepsilon_m = 0, \tag{10}$$

which leads to the solution for the α and β coefficients:

$$\alpha = -\frac{\delta_{kl}\varepsilon_m + \delta_m\varepsilon_{kl}}{\delta_{ij}\varepsilon_m + \delta_m\varepsilon_{ij}} \quad \text{and} \quad \beta = \frac{-\delta_{kl}\varepsilon_{ij} + \delta_{ij}\varepsilon_{kl}}{\delta_{ij}\varepsilon_m + \delta_m\varepsilon_{ij}} \tag{11}$$

Choosing these coefficients brings $\mathcal{L}_{kl,ij,m} = N^s_{r,kl} + b_{r,\mathcal{L}_{kl,ij,m}}$, with the new combined code and WL bias $b_{r,\mathcal{L}_{kl,ij,m}}$.

Since this approach takes benefit of the previously obtained information, the resulting combination has a lower carrier-to-noise level than the corresponding MW combination. The first two rows of Tables 3a and 3b gives the coefficients of $N^s_{r,\text{WL},65a}$ and the $N^s_{r,\text{WL},65b}$ ambiguity, as well as the carrier-to-noise ratio of the resulting combinations. The phase and code coefficients have very different order of magnitudes. They are related to the difference between the code and the phase noises. In this case, it is mandatory to take into account the correlation between the already fixed WL and the ones whose ambiguities are looked for. The correlation between the code and the phase measurements on each individual frequency is however neglected.

WL coefficients for $N^s_{r,\text{WL},65a}$ estimation						$\sigma_{N^s_{r,\text{WL},65a}}$ [0.01 cy]
$L_{\text{WL},5b5a}$	$L_{\text{WL},65b}$	C_1	C_{5a}	C_{5b}	C_6	
-2.897		$-8.500 \cdot 10^{-3}$				4.885
	-1.527	$4.481 \cdot 10^{-3}$				2.575
-2.326		$-6.994 \cdot 10^{-3}$	$-4.957 \cdot 10^{-3}$	$-5.319 \cdot 10^{-3}$	$-5.969 \cdot 10^{-3}$	4.366
	-1.419	$3.582 \cdot 10^{-3}$	$-2.998 \cdot 10^{-3}$	$-2.059 \cdot 10^{-3}$	$-0.268 \cdot 10^{-3}$	2.453

(a) $65a$ WL combination

WL coefficients for $N^s_{r,\text{WL},65b}$ estimation						$\sigma_{N^s_{r,\text{WL},65b}}$ [0.01 cy]
$L_{\text{WL},5b5a}$	$L_{\text{WL},65a}$	C_1	C_{5a}	C_{5b}	C_6	
-1.897		$-8.500 \cdot 10^{-3}$				4.885
	-0.655	$-2.934 \cdot 10^{-3}$				1.686
-1.326		$-6.994 \cdot 10^{-3}$	$-4.957 \cdot 10^{-3}$	$-5.319 \cdot 10^{-3}$	$-5.969 \cdot 10^{-3}$	2.453
	-0.659	$-2.689 \cdot 10^{-3}$	$0.666 \cdot 10^{-3}$	$0.177 \cdot 10^{-3}$	$-0.751 \cdot 10^{-3}$	1.660

(b) $65b$ WL combination

Table 3: Table of the α and β coefficients as per Equation (9) for the ionosphere-free geometry-free WL combinations with a non-ambiguous WL in order to estimation the $N^s_{r,\text{WL},65a}$ (resp. $N^s_{r,\text{WL},65b}$) ambiguities.

The observation problem to be solved in order to fix the ambiguities is the same as the one described by Equation (6), with a smaller carrier-to-noise ratio. Therefore, it is expected that the ambiguity fixing success rate is higher than the one obtained with the MW combination. An even smaller carrier-to-noise ratio can be obtained using all the n_C available code measurements. Equation (9) is transformed to:

$$\mathcal{L}_{kl,ij,m} = L_{\text{WL},kl} + \alpha \bar{L}_{\text{WL},ij} + \sum_{m=1}^{n_C} \beta_m \delta_m C_m, \tag{12}$$

and the conditions for a geometry-free and ionosphere-free combination read:

$$\delta_{kl} + \alpha\delta_{ij} + \sum_{m=1}^{n_C} \beta_m \delta_m = 0 \quad \text{and} \quad -\varepsilon_{kl} - \alpha\varepsilon_{ij} + \sum_{m=1}^{n_C} \beta_m \varepsilon_m = 0. \tag{13}$$

If at least two code measurements are taken into account in this combination, the number of parameters to be determined is bigger than the number of constraints. It is therefore possible to choose the α and β_m parameters in such a way that the resulting combination has the lowest possible carrier-to-noise ratio. To do so, it is first mandatory to compute the standard deviation of the carrier-to-noise ratio of the $\mathcal{L}_{kl,ij,m}$ combination:

$$\begin{aligned} \mathbb{V}\big(\mathcal{L}_{kl,ij,m}\big) &= \mathbb{V}\big(L_{\text{WL},kl}\big) + \alpha^2 \mathbb{V}\big(\bar{L}_{\text{WL},ij}\big) + 2\alpha \text{Cov}\big(L_{\text{WL},kl}, \bar{L}_{\text{WL},ij}\big) + \sum_{m=1}^{n_C} \beta_m^2 \mathbb{V}\big(C_m\big), \\ &= \sigma_L^2 \left[\frac{1}{\lambda_k^2} + \frac{1}{\lambda_l^2} + \alpha^2 \left(\frac{1}{\lambda_i^2} + \frac{1}{\lambda_j^2} \right) + 2\alpha \left(\frac{\varsigma_{ki} - \varsigma_{kj}}{\lambda_k^2} - \frac{\varsigma_{li} - \varsigma_{lj}}{\lambda_l^2} \right) \right] + \sigma_C^2 \sum_{m=1}^{n_C} \beta_m^2, \end{aligned} \tag{14}$$

with σ_L the carrier-to-noise ratio of the individual phase measurement expressed in meters, σ_C^2 the standard deviation of the code

measurement noise, ς_{ij} the Kronecker symbol defined by:

$$\varsigma_{ij} = \begin{cases} 0 \text{ if } i \neq j, \\ 1 \text{ if } i = j. \end{cases} \tag{15}$$

Finding the noise-optimal WL and code combination is recalled as the following optimisation problem:

$$\min_{\alpha,\beta_m} J(\alpha, \beta_m) = x^T P x + 2c^T x, \quad \text{such that } \; Ax = b, \tag{16}$$

with x the vector of the unknown parameters $x = [\alpha \quad \beta_1 \quad \cdots \quad \beta_m]^T$ and:

$$P = \begin{bmatrix} \sigma_L^2 \left(\frac{1}{\lambda_i^2} + \frac{1}{\lambda_j^2} \right) & & & \\ & \sigma_C^2 \frac{1}{\lambda_1^2} & (0) & \\ & & \ddots & \\ & (0) & & \sigma_C^2 \frac{1}{\lambda_m^2} \end{bmatrix}, \quad c = \begin{bmatrix} \sigma_L^2 \left(\frac{\varsigma_{ki} - \varsigma_{kj}}{\lambda_k^2} - \frac{\varsigma_{li} - \varsigma_{lj}}{\lambda_l^2} \right) \\ 0 \\ \vdots \\ 0 \end{bmatrix}, \tag{17}$$

$$A = \begin{bmatrix} \delta_{ij} & \delta_1 & \cdots & \delta_m \\ -\varepsilon_{ij} & \varepsilon_1 & \cdots & \varepsilon_m \end{bmatrix}, \quad b = \begin{bmatrix} -\delta_{kl} \\ \varepsilon_{kl} \end{bmatrix}. \tag{18}$$

The solution of this minimisation problem is given by:

$$x = P^{-1} \Big[A^T \big(A P^{-1} A^T \big)^{-1} \big(b + A P^{-1} c \big) - c \Big], \tag{19}$$

and the resulting coefficients are given by the last two rows of the Tables 3a and 3b.

To summarize, the first EWL ambiguity $N^s_{r,\text{WL},5b5a}$ is fixed, then it is possible to choose to fix the $N^s_{r,\text{WL},65a}$ ambiguity thanks to the already fixed $L_{\text{WL},5b5a}$ WL and then to fix the $N^s_{r,\text{WL},65b}$ ambiguity thanks to the already fixed $L_{\text{WL},65a}$ WL. On the other hand, it also possible to first fix the $N^s_{r,\text{WL},65b}$ ambiguity thanks to the already fixed $L_{\text{WL},5b5a}$ WL and then the $N^s_{r,\text{WL},65a}$ ambiguity thanks to the already fixed $L_{\text{WL},65b}$ WL. The Figure 1 depicts the two possible cascading strategies.

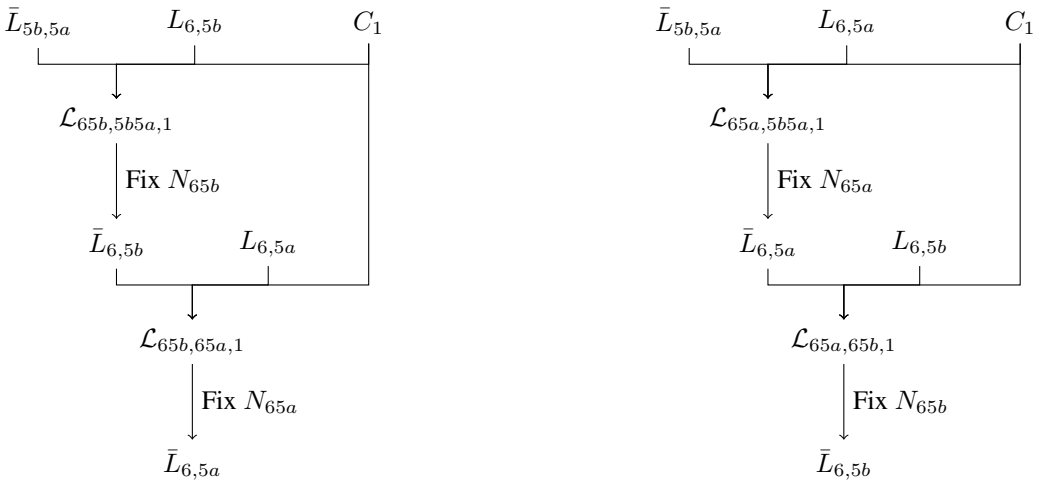

(a) Solving $N_{6,5b}$ first

(b) Solving $N_{6,5a}$ first

Figure 1: Galileo cascading schemes

III Fixing the Widelane Ambiguities

As shown in the Table 2, the Melbourne-Wübbena combination between the upper L-band (f_i) and the lower L-band (f_j) has a noise of almost half a cycle, and the corresponding WL ambiguity cannot be fixed. The same noise-optimal combinations as described in Equations (9) and (12), using one or more of the EWL already fixed, can be performed. Although the carrier-to-noise ratio of these combinations are much smaller than the one of the corresponding MW, it remains slightly bigger than a quarter of a cycle, thus preventing the Algorithm 1 from being able to fix the ambiguities. The solution would oscillate between two integer values.

1 The widelanes cascading scheme

An improvement of the intrinsic weakness of the previously introduced cascading scheme would be to rely on a geometry-free combination instead of a ionosphere-free geometry-free one. Let I^L_{EWL} be the indexes of the fixed EWL from the lower band frequencies. The aim is to build a linear combination with an ambiguous WL $L_{\text{WL},ij}$, and the previously fixed EWL combinations $\bar{L}_{\text{WL},i_k j_k},\ (i_k, j_k)_{k\in I^L_{\text{EWL}}}$. This combination reads:

$$\begin{aligned}\mathcal{L}_{\text{GF},ij,I^L_{\text{EWL}}} &= \alpha L_{\text{WL},ij} + \sum_{k\in I^L_{\text{EWL}}} \beta_k \bar{L}_{\text{WL},i_k j_k},\\ &= \alpha\Big(\delta_{ij} D^s_r - \varepsilon_{ij} e^s + b_{r,\text{WL},ij} + N^s_{r,ij}\Big) + \sum_{k\in I^L_{\text{EWL}}} \beta_k \Big(\delta_{i_k j_k} D^s_r - \varepsilon_{i_k j_k} e^s + b_{r,\text{WL},i_k j_k}\Big),\end{aligned} \tag{20}$$

It is possible to obtain a geometry-free linear combination by imposing the following constraints:

$$\alpha\ \delta_{ij} + \sum_{k\in I^L_{\text{EWL}}} \beta_k \delta i_k, j_k = 0 \quad \text{and } \alpha\ \varepsilon_{ij} + \sum_{k\in I^L_{\text{EWL}}} \beta_k \varepsilon_{i_k,j_k} = -1. \tag{21}$$

With these constraints, the combination reads:

$$\mathcal{L}_{\text{GF},ij,I^L_{\text{EWL}}} = e^s + \alpha\big(N^s_{r,\text{WL},ij} + b_{r,\text{GF,WL},ij}\big), \tag{22}$$

with $b_{r,\text{GF,WL},ij}$ the geometry-free phase bias.

As opposed to the ionosphere-free combination involving only two WL presented in the reference Laurichesse and Langley (2015), the proposed combination is geometry-free and uses more than two WL combinations. The system described by Equation (20) is underdetermined. Therefore, the unknowns α and β_k are chosen in order to minimize the noise of the combination, that is expressed taking into account the correlations of the WL sharing a common frequency:

$$\begin{aligned}\mathbb{V}\big(\mathcal{L}_{\text{GF},ij,m}\big) &= \alpha^2 \mathbb{V}\big(L_{\text{WL},ij}\big) + \sum_{k\in I^L_{\text{EWL}}} \beta_k^2 \mathbb{V}\big(\bar{L}_{\text{WL},i_k j_k}\big)\\ &\quad + 2\alpha \sum_{k\in I^L_{\text{EWL}}} \beta_k \text{Cov}\big(L_{\text{WL},ij}, \bar{L}_{\text{WL},i_k j_k}\big) + 2 \sum_{(k,l)\in I^L_{\text{EWL}}} \beta_k \beta_l \text{Cov}\big(\bar{L}_{\text{WL},i_k j_k}, \bar{L}_{\text{WL},i_l j_l}\big),\\ &= \sigma_L^2 \left[\alpha^2 \left(\frac{1}{\lambda_i^2} + \frac{1}{\lambda_j^2}\right) + \sum_{k\in I^L_{\text{EWL}}} \beta_k^2 \left(\frac{1}{\lambda_{i_k}^2} + \frac{1}{\lambda_{j_k}^2}\right)\right.\\ &\quad \left. + 2\alpha \sum_{k\in I^L_{\text{EWL}}} \beta_k \left(\frac{\varsigma_{ii_k} - \varsigma_{ij_k}}{\lambda_i^2} + \frac{\varsigma_{jj_k} - \varsigma_{ji_k}}{\lambda_j^2}\right) + 2 \sum_{(k,l)\in I^L_{\text{EWL}}} \beta_k \beta_l \left(\frac{\varsigma_{i_k i_l} - \varsigma_{i_k j_l}}{\lambda_{i_k}^2} + \frac{\varsigma_{j_k j_l} - \varsigma_{j_k i_l}}{\lambda_{j_k}^2}\right)\right],\end{aligned} \tag{23}$$

with the Kronecker symbol ς_{ij} defined as in the previous section. Finding the noise-optimal multi-widelanes geometry-free combination is recast as the following minimisation problem:

$$\min_x x^T P x \quad \text{such that } Ax = b, \tag{24}$$

WL coefficients for $\mathcal{L}_{\text{GF},5a1}$ estimation [m^{-1}]				$\sqrt{\mathbb{V}(\mathcal{L}_{\text{GF},5a1})}$ [cm]
$L_{\text{WL},5a1}$	$\bar{L}_{\text{WL},5b5a}$	$\bar{L}_{\text{WL},65a}$	$\bar{L}_{\text{WL},65b}$	
2.417		9.464	−0.052	15.11
2.417	−9.464		9.412	15.11
2.417	−0.052	9.412		15.11

(a)

WL coefficients for $\mathcal{L}_{\text{GF},5b1}$ estimation [m^{-1}]				$\sqrt{\mathbb{V}(\mathcal{L}_{\text{GF},5b1})}$ [cm]
$L_{\text{WL},5b1}$	$\bar{L}_{\text{WL},5b5a}$	$\bar{L}_{\text{WL},65a}$	$\bar{L}_{\text{WL},65b}$	
2.417		7.047	2.366	15.11
2.417	−7.047		9.412	15.11
2.417	2.366	9.412		15.11

(b)

WL coefficients for $\mathcal{L}_{\text{GF},61}$ estimation [m^{-1}]				$\sqrt{\mathbb{V}(\mathcal{L}_{\text{GF},61})}$ [cm]
$L_{\text{WL},61}$	$\bar{L}_{\text{WL},5b5a}$	$\bar{L}_{\text{WL},65a}$	$\bar{L}_{\text{WL},65b}$	
2.417		7.047	−0.052	15.11
2.417	−7.047		6.995	15.11
2.417	−0.052	6.995		15.11

(c)

Table 4: Table of the α and β coefficients as per Equation (20) for the geometry-free WL combinations with a non-ambiguous WL. The noise ratio of these combinations are also given.

with the unknown vector x being defined as: $x = [\alpha \quad \beta_1 \quad \beta_2 \quad \cdots]^T$ and:

$$P = \sigma_L^2 \begin{bmatrix} \frac{1}{\lambda_i^2} + \frac{1}{\lambda_j^2} & \frac{\varsigma_{ii_1} - \varsigma_{ij_1}}{\lambda_i^2} + \frac{\varsigma_{jj_1} - \varsigma_{ji_1}}{\lambda_j^2} & \frac{\varsigma_{ii_2} - \varsigma_{ij_2}}{\lambda_i^2} + \frac{\varsigma_{jj_2} - \varsigma_{ji_2}}{\lambda_j^2} & \cdots \\ & \frac{1}{\lambda_{i_1}^2} + \frac{1}{\lambda_{j_1}^2} & \frac{\varsigma_{i_1i_2} - \varsigma_{i_1j_2}}{\lambda_{i_1}^2} + \frac{\varsigma_{j_1j_2} - \varsigma_{j_1i_2}}{\lambda_{j_1}^2} & \\ & & \ddots & \\ \text{(sym.)} & & & \ddots \end{bmatrix}, \tag{25}$$

$$A = \begin{bmatrix} \delta_{ij} & \delta_{i_1,j_1} & \delta_{i_2,j_2} & \cdots \\ \varepsilon_{ij} & \varepsilon_{i_1,j_1} & \varepsilon_{i_2,j_2} & \cdots \end{bmatrix}, \quad \text{and} \quad b = \begin{bmatrix} 0 \\ -1 \end{bmatrix}. \tag{26}$$

The minimisation problem described by Equation (24) is an underdetermined weighted least squares problem. Its solution is thus given by:

$$x = P^{-1}A^T\left(AP^{-1}A^T\right)^{-1}b. \tag{27}$$

The proposed geometry-free combination is applied with the non-ambiguous EWL already fixed by the previous cascading scheme, and an ambiguous WL. It has to be noted that the three EWL cannot be used together since the matrix P would become rank-deficient and would not be invertible. A dimensional analysis shows that the coefficients are homogeneous to the inverse of a distance. The Tables 4a, 4b and 4c give the coefficients for the geometry-free WL coefficients, as well as its noise level, for the three Galileo remaining WL, $L_{\text{WL},5a1}$, $L_{\text{WL},5b1}$ and $L_{\text{WL},61}$ respectively. The noise level is mostly affected by the ambiguous WL noise. Therefore, all the combination have the same standard deviation.

It is no longer possible to estimate the WL ambiguities in a snapshot mode. A Kalman filter has to be set up to estimate the ambiguities together with the ionospheric elongation. Nevertheless, this filter is less cumbersome than a Kalman filter dedicated to the estimation of the position of a receiver. As the WL combination is ambiguous, it is mandatory to add an absolute geometry-free code measurement so that the ambiguities can be estimated. A geometry-free Doppler measurement is also added to enforce the ionosphere elongation estimation. Geometry-free code, Doppler and WL biases have to be added.

Assuming that n_S satellites are in view of the receiver, the state vector x_{KF} of the filter consists in the slant ionospheric elongation in the receiver-satellite direction as well as its drift, denoted e^s and $\dot{e}^s$ respectively for the satellite s, the WL ambiguity $N^s_{r,\text{WL},ij}$ as well as the geometry-free code bias $b_{r,\text{GF},C_{ij}}$, Doppler bias $b_{r,\text{GF},D_{ij}}$ and WL bias b_{r,WL,i_kj_k}.

The Kalman filter is corrected by the following measures:

- a geometry-free code combination for each satellite in view:

$$C^s_{\text{GF},ij} = \frac{C^s_i - C^s_j}{\gamma_i - \gamma_j} = e^s + \frac{b_{r,C_i} - b_{r,C_j}}{\gamma_i - \gamma_j} = e^s + b_{r,\text{GF},C_{ij}}, \tag{28}$$

- a geometry-free Doppler combination for each satellite in view:

$$D^s_{\text{GF},ij} = -\frac{D^s_i - D^s_j}{\gamma_i - \gamma_j} = \dot{e}^s - \frac{b_{r,D_i} - b_{r,D_j}}{\gamma_i - \gamma_j} = \dot{e}^s + b_{r,\text{GF},D_{ij}}, \tag{29}$$

- the previously computed geometry-free WL combination given by Equation (22) for each satellite in view.

All the unknowns cannot be observed simultaneously from the three measurements, $C_{\text{GF},ij}$ and $D_{\text{GF},ij}$ and $\mathcal{L}_{\text{GF},ij,I^L_{\text{EWL}}}$. One way to address this issue is to remove one state and define the new states with a biased ionospheric elongation: for $s \in \{1, \ldots, n_S\}$:

$$\begin{cases} \tilde{e}^s & = e^s + b_{r,\text{GF},C_{ij}}, \\ \dot{\tilde{e}}^s & = \dot{e}^s + \dot{b}_{r,\text{GF},C_{ij}}, \\ \tilde{b}_{r,\text{WL},i_k j_k} & = b_{r,GF,\text{WL},i_k j_k} - \alpha^{-1} b_{r,\text{GF},C_{ij}}, \\ \tilde{b}_{r,\text{GF},D_{ij}} & = b_{r,\text{GF},D_{ij}} - \dot{b}_{r,\text{GF},C_{ij}}, \end{cases} \tag{30}$$

with $\dot{b}_{r,\text{GF},C_{ij}}$ the drift of the geometry-free code bias. The state vector x_k of the Kalman filter at epoch t_k is thus defined by:

$$x_{\text{KF}} = \begin{bmatrix} \tilde{e}^{s_1} & \cdots & \tilde{e}^{s_{n_S}} & \dot{\tilde{e}}^{s_1} & \cdots & \dot{\tilde{e}}^{s_{n_S}} & N^1_{r,\text{WL},ij} & \cdots & N^{n_S}_{r,\text{WL},ij} & \tilde{b}_{r,\text{GF},D_{ij}} & \tilde{b}_{r,\text{GF,WL},ij} \end{bmatrix}^T \tag{31}$$

The propagation model assumes that all the states are constant, except the ionospheric elongations which follow an explicit Euler scheme. The ionospheric elongation and its drift at time $k+1$ are linked to the one at the epoch k by:

$$\forall s \in \{1, \ldots, n_S\}, \begin{cases} \tilde{e}^s_{k+1} = \tilde{e}^s_k + \Delta t \, \dot{\tilde{e}}^s_k + w_{e,k}, \\ \dot{\tilde{e}}^s_{k+1} = \dot{\tilde{e}}^s_k + w_{\dot{e},k} \end{cases} \tag{32}$$

with Δt the time interval between two epochs, $w_{e,k}$ and $w_{\dot{e},k}$ the ionospheric elongation and drift process noises respectively whose variance are given by q_e and $q_{\dot{e}}$. The propagation equation is thus given in matrix form by:

$$x_{k+1} = \begin{bmatrix} \boldsymbol{I}_{n_S} & \Delta t \, \boldsymbol{I}_{n_S} & \boldsymbol{0}_{n_S} & \boldsymbol{0}_{n_S \times 2} \\ \boldsymbol{0}_{n_S} & \boldsymbol{I}_{n_S} & \boldsymbol{0}_{n_S} & \boldsymbol{0}_{n_S \times 2} \\ \boldsymbol{0}_{n_S} & \boldsymbol{0}_{n_S} & \boldsymbol{I}_{n_S} & \boldsymbol{0}_{n_S \times 2} \\ \boldsymbol{0}_{2 \times n_S} & \boldsymbol{0}_{2 \times n_S} & \boldsymbol{0}_{2 \times n_S} & \boldsymbol{I}_2 \end{bmatrix} x_k + w_k, \tag{33}$$

where w_k encapsulates the process noises for all the elements of the state vector, $\boldsymbol{I}_{n_S}$ is the identity matrix of size n_S, $\boldsymbol{0}_{n_S}$ is the null matrix of size n_S, $\boldsymbol{1}_{p \times q}$ is a matrix of size $p \times q$ filled with 1.

The measure vector filled with the code, Doppler and WL geometry-free measurements at time t_k is denoted y_k and the observation equations are given by:

$$\begin{cases} C^{s_i}_{\text{GF},ij} = \tilde{e}^{s_i} + v_{C,k} \\ D^{s_i}_{\text{GF},ij} = \dot{\tilde{e}}^{s_i} + \tilde{b}_{r,\text{GF},D_{ij}} + v_{D,k}, \\ \mathcal{L}^{s_i}_{\text{GF},ij,I^L_{\text{EWL}}} = \tilde{e}^{s_i} + \alpha \left(N^{s_i}_{r,\text{WL},ij} + \tilde{b}_{r,\text{GF,WL},ij} \right) + v_{\text{WL},k}, \end{cases} \tag{34}$$

with $v_{C,k}$, $v_{D,k}$ and $v_{\text{WL},k}$ the geometry-free code, Doppler and WL measure noises at epoch t_k respectively. In matrix form, the observation equation is recast as:

$$y_k = \begin{bmatrix} \boldsymbol{I}_{n_S} & \boldsymbol{0}_{n_S} & \boldsymbol{0}_{n_S} & \boldsymbol{0}_{n_S \times 1} & \boldsymbol{0}_{n_S \times 1} \\ \boldsymbol{0}_{n_S} & \boldsymbol{I}_{n_S} & \boldsymbol{0}_{n_S} & \boldsymbol{1}_{n_S \times 1} & \boldsymbol{0}_{n_S \times 1} \\ \boldsymbol{I}_{n_S} & \boldsymbol{0}_{n_S} & \alpha \boldsymbol{I}_{n_S} & \boldsymbol{0}_{n_S \times 1} & \alpha \boldsymbol{1}_{n_S \times 1} \end{bmatrix} x_k + v_k, \tag{35}$$

where v_k encapsulated the measure noise.

The integer constraint is applied with a bootstrap method, as described in (Teunissen and Montenbruck, 2017, Chapter 20), after the update step of the Kalman filter. Once the ambiguity is fixed, its corresponding covariance terms are forced to 0. To do so, it is required to define a floating ambiguity covariance and a integer gap thresholds τ_P and τ_N respectively. If at a given epoch the estimated covariance is smaller than τ_P, and the distance between the estimated floating ambiguity and the nearest integer is smaller than τ_N, the ambiguity is fixed to the nearest integer.

2 Processing summary

For the Galileo constellation, the cascading algorithm follows these steps:

1. build the Melbourne-Wübbena combination with the L_{5b} and L_{5a} phase measurements,
2. solve for the integer $N_{\text{WL},5b5a}$ WL ambiguity and build the not ambiguous $\bar{L}_{\text{WL},5b5a}$ WL combination,
3. build the new combination $\mathcal{L}_{65b,5b5a,1}$ with the already fixed $\bar{L}_{\text{WL},5b5a}$, the ambiguous WL $L_{\text{WL},6-5b}$,
4. solve for the integer $N_{\text{WL},65b}$ WL ambiguity and build the not ambiguous $\bar{L}_{\text{WL},6-5b}$ WL combination,
5. build the new combination $\mathcal{L}_{65a,65b,1}$ with the already fixed $\bar{L}_{\text{WL},65b}$, the ambiguous WL $L_{\text{WL},65a}$,
6. solve for the integer $N_{\text{WL},65a}$ WL ambiguity and build the not ambiguous $\bar{L}_{\text{WL},65a}$ WL combination,
7. build the geometry-free optimized WL $L_{16}^{\alpha,\beta}$ using all the previously fixed EWL,
8. estimate the ambiguity with the Kalman Filter using the geometry-free optimized WL, the geometry free code and Doppler as measurements.

IV Case study, experiment and expected results

The effectiveness of the proposed method is evaluated in this section within both static and dynamic contexts. The case considered in this study at the following ones:

1. case A: the reference station TLSE00FRA with data from the Day of Year (DOY) 2023-345 (December 11$^{\text{th}}$, 2023) at a 1 Hz sample rate,
2. case B: a dynamic run around and within the city center of Toulouse, France (the same case as the one presented in Gazzino et al. (2023)). The car was equipped with a Novatel antenna mounted on the roof and connected to a signal splitter. One signal path directed to a ProPack 6 receiver and a Novatel Inertial Measurement Unit (IMU) for computing a reference trajectory, while the other path fed a Septentrio PolaRx5 receiver, whose data were used to estimate the car's position in this study. The lever arms from the IMU to the antenna were calibrated to centimeter-level accuracy. Notably, measurements were sampled at 10 Hz, differing from the typical 1 Hz sampling rate in the navigation community.

The proposed cascading approach is applied in order to fix the Galileo EWL ambiguities with Algorithm 1. The percentage of epochs for which 100 % of the ambiguities are fixed is presented in Table 5. This Table first shows the fixation success rates for each EWL ambiguities fixed independently from each other by means of the classical Melbourne-Wübbena combination. The success rates for the proposed noise-optimal combination of already fixed WL and code measurements are then presented in the subsequent tables. The percentages displayed clearly demonstrate that reducing the noise of the combination leads to an increase of the percentage of time where all the ambiguities are fixed. This increase is more significant for the dynamic case (case B).

Case	Case A			Case B		
	$N^s_{r,\text{WL},5b5a}$	$N^s_{r,\text{WL},65a}$	$N^s_{r,\text{WL},65b}$	$N^s_{r,\text{WL},5b5a}$	$N^s_{r,\text{WL},65a}$	$N^s_{r,\text{WL},65b}$
Fixation Percentage with the MW combination	100 %	87.65 %	98.13 %	95.03%	80.47 %	87.52%

(a)

Fixation percentage for $N^s_{\textbf{EWL},65a}$	Case A	Case B
Melbourne-Wübbena	87.65 %	80.47 %
$\mathcal{L}_{65a,5b5a,C_1}$ with $N^s_{\text{WL},5b5a}$ and C_1	99.35 %	87.53 %
$\mathcal{L}_{65a,5b5a,C_n}$ with $N^s_{\text{WL},5b5a}$ and all C_n	99.85 %	90.77 %
$\mathcal{L}_{65a,65b,C_1}$ with $N^s_{\text{WL},65b}$ and C_1	100 %	96.97 %
$\mathcal{L}_{65a,65b,C_n}$ with $N^s_{\text{WL},65b}$ and all C_n	100 %	97.03 %

(b)

Fixation percentage for $N^s_{\textbf{EWL},65b}$	Case A	Case B
Melbourne-Wübbena	98.13 %	80.47 %
$\mathcal{L}_{65b,5b5a,C_1}$ with $N^s_{\text{WL},5b5a}$ and C_1	99.35 %	87.57 %
$\mathcal{L}_{65b,5b5a,C_n}$ with $N^s_{\text{WL},5b5a}$ and all C_n	99.85 %	90.85 %
$\mathcal{L}_{65b,65a,C_1}$ with $N^s_{\text{WL},65b}$ and C_1	100 %	98.21 %
$\mathcal{L}_{65b,65a,C_n}$ with $N^s_{\text{WL},65b}$ and all C_n	100 %	98.24 %

(c)

Table 5: Percentage of the time for which all the extra WL ambiguities are fixed for all the satellites in view. Table 5a shows results with the classical Melbourne-Wübbena strategy. Tables 5b and 5c depict the success rate for the new proposed noise-optimal combinations and the resulting cascading fixation strategy.

The benefit of reducing the noise of the combination can be shown on the post-fit residuals histograms after having fixed the ambiguities as on Figure 2 for the case B. Note that the situation is the same for the case A, with the differences between each combination less visible since the measures are of good quality. For the histograms on the Figure 2a corresponding to the combinations with minimal noise, the residuals are more concentrated around 0, and the estimated receiver bias values on Figure 2b are less spread around they mean value, hence the higher fixation rate. For readibility reasons, the phase biases have been shifted by an integer value. The effect of the multipath on the performance has not been assessed.

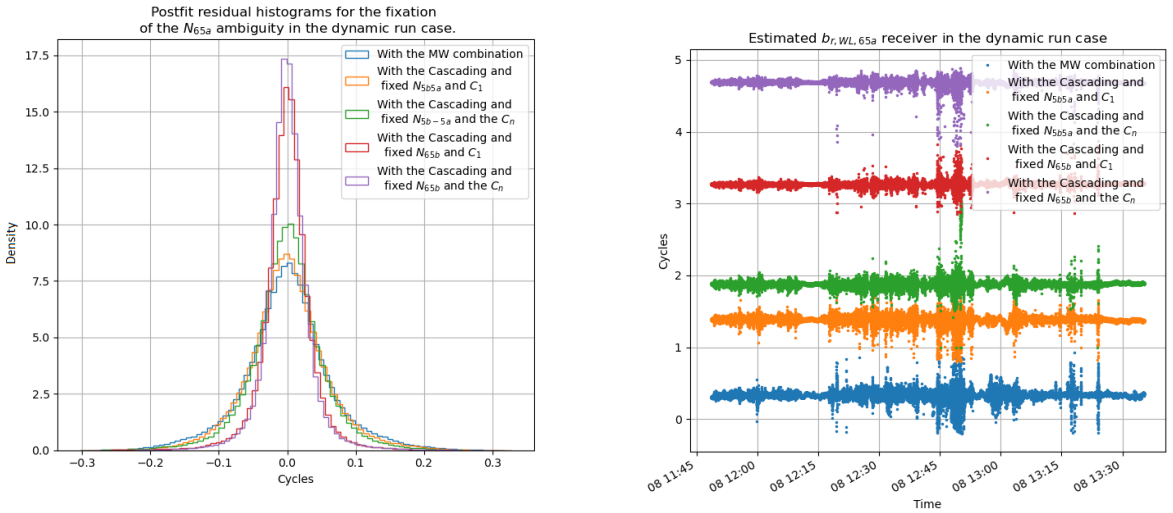

(a) Postfix ambiguity residuals

(b) Estimated receiver bias

Figure 2: Postfix ambiguity residuals and estimated receiver bias for the $N^s_{\text{EWL},65a}$ in case B for all the presented combinations.

As described in the Section II.2, the instantaneous ambiguity fixing problem is rank deficient. The estimated receiver bias may exhibit integer jumps while the estimated ambiguity jump in the opposite direction. The Figure 3a depicts the receiver bias estimated together with the $N^s_{r,\text{EWL},65a}$ ambiguity. Frequent cycle slips occur. Applying the cycle slips detection algorithm described in Subirana et al. (2013), and correcting the receiver bias by the estimated jumps lead to the receiver bias illustrated on Figure 3b.

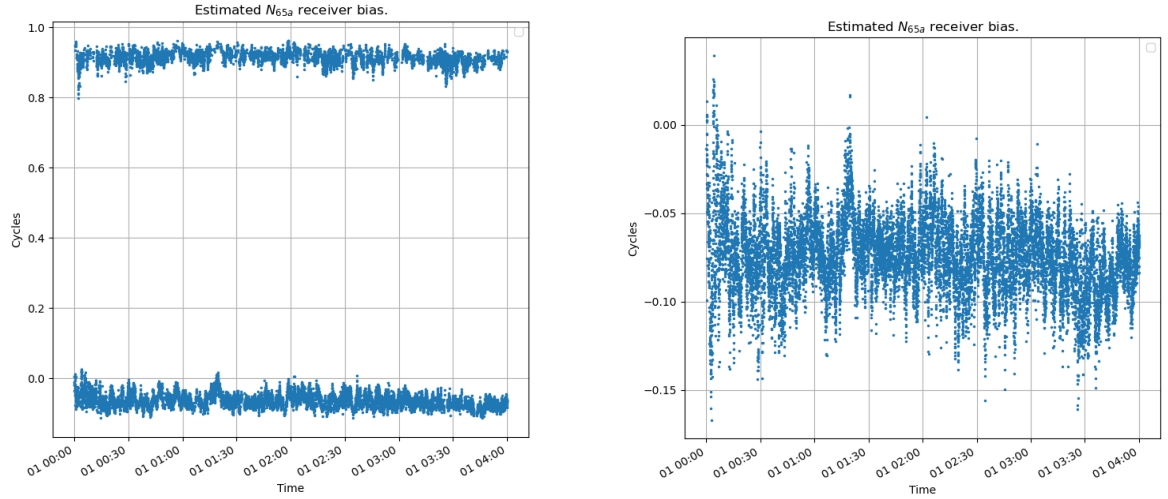

(a) Without cycle slips detection

(b) After having estimated and corrected the cycle slips

Figure 3: Estimated receiver phase bias $b_{r,65a}$ obtained during the fixation process described in Algorithm 1 for the $N^s_{r,\text{EWL},65a}$ ambiguity in the case A.

Applying the Algorithm 1 on the noise-optimal combination of already fixed WL and code measurements in order to fix the $N^s_{r,\mathrm{WL},5a1}$, the $N^s_{r,\mathrm{WL},5b1}$, and the $N^s_{r,\mathrm{WL},61}$ WL leads to very low fixing sucess rates of around 30 %. This is mainly due to the fact that the floating ambiguities for satellites at low elevation have a higher carrier-to-noise ratio than for the ones at high elevation. Therefore, these low-elevated satellites prevent the receiver phase bias from being well estimated, and the ambiguities of the high-elevated satellites cannot be fixed. To illustrate this effect, an analysis of the percentage of time where all the ambiguities for the satellites in view are fixed depending of the elevation cutoff angle. This percentage is displayed on the Figure 4. The higher the angle cutoff, the higher the percentage of time where all the ambiguities are fixed. The following conclusion can be drawn from the presented figures. When the elevation mask is too high, the percentage of epochs for which at least one satellite measure remains falls down. Therefore the Kalman filtering technique presented in Section III has to be used.

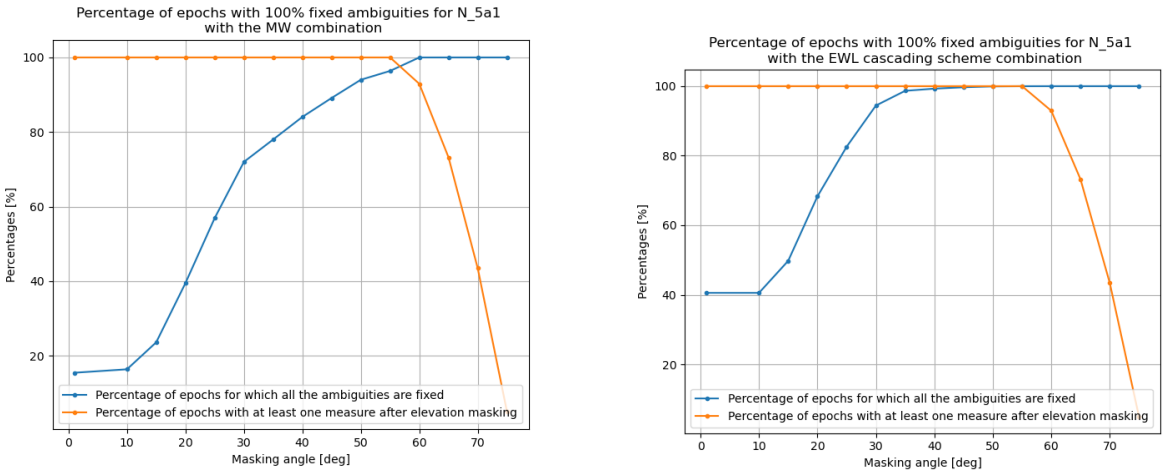

(a) Melbourne-Wübbena approach

(b) Waterfall approach

Figure 4: Percentage of the epochs for which all the ambiguities for the satellites in view are fixed and percentage of the epochs for which at least one measurement remains as a function of the angle elevation cutoff.

The geometry-free Kalman filter is thus implemented in order to estimate the float $N^s_{r,\mathrm{WL},5a1}$, the $N^s_{r,\mathrm{WL},5b1}$ and the $N^s_{r,\mathrm{WL},61}$ ambiguities, and fed with the noise-optimal WL geometry-free combination described by Equation (20). Table 6 gives the settings applied to the filter. The ambiguity fixing success rate is counted as the number of epochs for which the ambiguity variance is set to 0 for all the visible satellites. Table 7 gives the ambiguity success rate for the three WL ambiguity estimation and fixing process in the case A. It has to be noted that the complexity of this filter is largely reduced with respect to a filter that encompasses the receiver position and velocity.

Parameter	Initial noise	Process noise
e^s	5 m	0
$\dot{e}^s$	1 m/s	10^{-5} m/s
$N^s_{r,\mathrm{WL},ij}$	5 cy	1 cy
$\tilde{b}_{r,\mathrm{GF},D_{ij}}$	10^8 m/s	1 m/s
$\tilde{b}_{r,\mathrm{GF,WL},ij}$	10^8 cy	1 cy

Table 6: Geometry-free Kalman filter settings for the estimation of the ionosphere elongation and the WL ambiguity.

Case	Case A			Case B		
	$N^s_{r,\mathrm{WL},5a1}$	$N^s_{r,\mathrm{WL},5b1}$	$N^s_{r,\mathrm{WL},61}$	$N^s_{r,\mathrm{WL},5a1}$	$N^s_{r,\mathrm{WL},5b1}$	$N^s_{r,\mathrm{WL},61}$
Fixation Percentage with the Kalman filter	99.146 %	99.062 %	99.146 %	97.11%	96.23 %	97.22%

Table 7: Percentage of the time for which all the WL ambiguities are fixed for all the satellites in view, computed with the geometry-free Kalman filter.

The rover position is estimated with a Kalman filter, whose state vector includes the receiver coordinates, the atmospheric delays,

and the receiver electronic biases. Since the EWL and WL ambiguities have been computed beforehand, the unambiguous carrier phase measurements can be taken into account along with the code and Doppler measurements. A Kalman filter dealing with the ambiguous phase measurements is set up for comparison. In this second filter, the ambiguities are estimated using the frequency combinations presented in Laurichesse and Langley (2015). Note that the N_1 ambiguity is not solved. The graphs of the Figure 5 expose the error of the TLSE station position estimation in the East and North directions. The blue curves are the one obtained by the filter implementing the proposed cascading scheme and the orange ones are computed with the traditional filter. The filtered have been periodically restarted in order to study the convergence phase. The proposed approach leads to smaller convergence times with respect to the traditional approach.

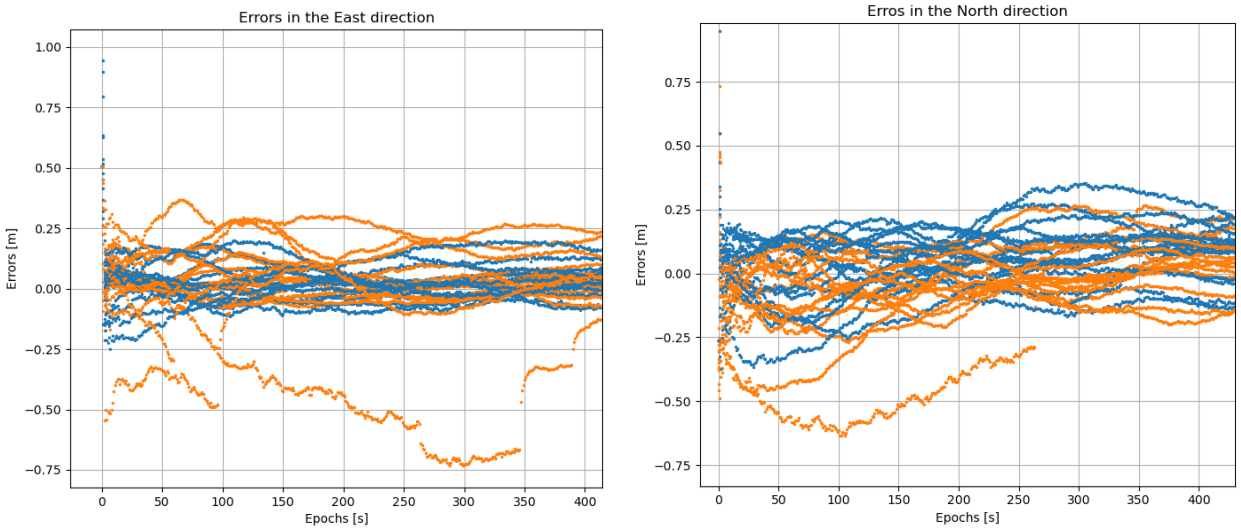

(a) Errors in the East direction

(b) Errors in the North direction

Figure 5: Positioning errors in the East and North directions for the TLSE station. The blue curves are the one obtained by the filter implementing the proposed cascading scheme and the orange ones are computed with the traditional filter.

The reduction of the convergence time can also be checked on the position covariance estimation as depicted on the Figure 6. The curves are the trace of the estimated position covariance matrix, either with the proposed cascading scheme (in blue) and with the traditional filter. The blue curves are below the orange ones, which means that the position converges more rapidly with the approach described in this article.

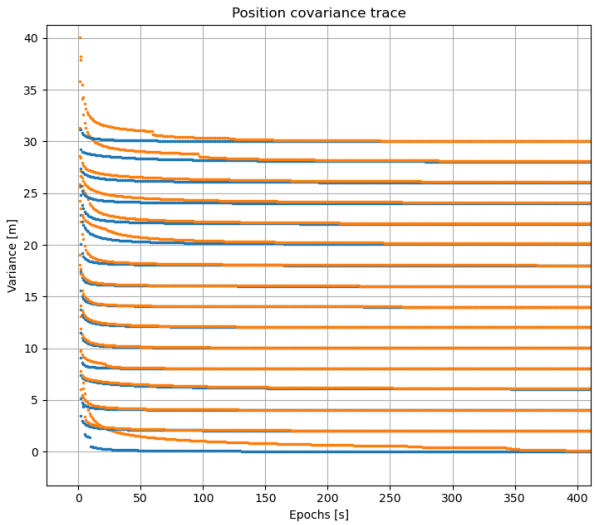

Figure 6: Evolution of the trace of the estimated position covariance matrix for several runs. The curves are shifted by integer values for readability reasons. The blue curves are the one obtained by the filter implementing the proposed cascading scheme and the orange ones are computed with the traditional filter.

CONCLUSION

The method described in this article takes advantage of the Galileo constellation frequency plan in order to instantaneously fix some carrier-phase ambiguities. The small frequency gap of the two signals in the E5-band is of great interest because of the small carrier-to-noise ratio of the phase combination. More specifically, the Melbourne-Wübbena combination that is traditionnaly employed for cycle-slips detection, is used here to let the ambiguities appear. A dedicated algorithm then isolates the ambiguities of each satellite in view from the receiver bias. The same method can be applied for the combination of signals between the E5 and E6 band. By optimizing the use of these frequencies, we have achieved significant improvements in the ambiguity fixing rate in single-epoch mode. A noise analysis has been conducted to choose the best combinations, thus introducing new combinations besides the ones classically used in the GNSS domain.

The phase combinations between the lower and upper L-band are too noisy for the previously method to work properly. Therefore, a new geometry-free WL combination is proposed. The ambiguities and the ionosphere elongation are estimated in the same Kalman filter. This filter has a simple form and reduce complexity with respect to a conventional filter dedicated to position estimation, and a fast convergence toward the integer values of the ambiguities. The resulting phase measurements are not ambiguous anymore, and they can therefore be used in order to estimate the position of a receiver. The convergence of the solution is also increased thanks to the proposed method.

Given the similarities in the signal structure and frequencies among different GNSS constellations, it is reasonable expect that our cascading approach can be extended to other systems. Future work should explore the application of this method to other constellations, particularly Beidou, which offers a comparable multi-frequency capability. Besides this, this work can open the door for the frequency plan definition of future satellite navigation systems, as for the upcoming Low Earth Orbit constellations. A recommendation for the future of the satellite navigation systems would be to fill the gaps between the frequencies. A large frequency difference is meaningful for ionosphere-free and geometry-free combinations. However, small frequencies differences are of high interest for instantaneous widelane ambiguity fixation.

One limitation of our approach lies in the ambiguity resolution method. Satellites at low elevation angles are noisier, leading to a butterfly effect. An initial approach is to exclude low-elevation satellites. Alternatively, we could turn toward robust estimation by weighting the measurements on an elevation basis to avoid losing too many satellites, while still emphasizing the less noisy measurements. This effect will be strengthened in the upcoming years because of the high geomagnetic activity due to the beginning of a new solar cycle. The ionospheric delay will grow significantly, in particular the second order terms. The ionosphere and ambiguity Kalman filter will have to be tuned again to cope with such effects.

ACKNOWLEDGEMENTS

The authors would like to thank Denis Laurichesse for its incredible contribution to the navigation field and specifically the precise point positioning area, as well as its kindness and its trust. The authors wish also to thank Mrs Alissa Kouraeva for her review of the manuscript.

REFERENCES

Bezmenov, I., Blinov, I., Naumov, A., and Pasynok, S. (2019). An algorithm for cycle-slip detection in a melbourne–wübbena combination formed of code and carrier phase gnss measurements. Measurement Techniques, 62.

Cocard, M., Bourgon, S., Kamali, O., and Collins, P. (2008). A systematic investigation of optimal carrier-phase combinations for modernized triple-frequency gps. Journal of Geodesy, 82:555–564.

Gazzino, C., Blot, A., Bernadotte, E., Jayle, T., Laymand, M., Lelarge, N., Lacabanne, A., and Laurichesse, D. (2023). The cnes solutions for improving the positioning accuracy with post-processed phase biases, a snapshot mode, and high-frequency doppler measurements embedded in recent advances of the ppp-wizard demonstrator. Remote Sensing, 15(17):4231.

Groves, P. D. (2008). Principles of GNSS, Inertial, and Multisensor Integrated Navigation Systems: Artech House. Inc. Boston.

Ji, S., Liu, G., Weng, D., Wang, Z., He, K., and Chen, W. (2022). Single-epoch ambiguity resolution of a large-scale cors network with multi-frequency and multi-constellation gnss. Remote Sensing, 14:3819.

Kaplan, E. D. and Hegarty, C. J. (2006). Understanding GPS - Principles and Applications, Second Edition. Artech House. Inc., MA.

Laurichesse, D. (2011). The cnes real-time ppp with undifferenced integer ambiguity resolution demonstrator. In Proceedings of the 24th International Technical Meeting of The Satellite Division of the Institute of Navigation (ION GNSS 2011), pages 654–662.

Laurichesse, D. (2012). Phase biases estimation for undifferenced ambiguity resolution. In PPP-RTK & Open Standards Symposium, pages 12–13.

Laurichesse, D. and Banville, S. (2018). Innovation: Instantaneous centimeter-level multi-frequency precise point positioning. GPS World, 4.

Laurichesse, D. and Langley, R. (2015). Handling the biases for improved triple-frequency ppp convergence. GPS World, 26(4).

Laurichesse, D. and Privat, A. (2015). An open-source ppp client implementation for the cnes ppp-wizard demonstrator. In Proceedings of the 28th International Technical Meeting of the Satellite Division of The Institute of Navigation (ION GNSS+ 2015), pages 2780–2789.

Li, B., Zhang, Z., Miao, W., and Chen, G. (2020). Improved precise positioning with bds-3 quad-frequency signals. Satellite Navigation, 1.

Liu, T., Chen, H., Chen, Q., Jiang, W., Laurichesse, D., An, X., and Geng, T. (2021). Characteristics of phase bias from cnes and its application in multi-frequency and multi-gnss precise point positioning with ambiguity resolution. GPS Solutions, 25:1–13.

Melbourne, W. G. (1985). The case for ranging in gps-based geodetic systems. In Proceedings of the first international symposium on precise positioning with the Global Positioning System, pages 373–386. US Department of Commerce Rockville, Maryland.

Subirana, J. S., Zornoza, J. J., and Hernandez-Pajares, M. (2013). Gnss data processing, vol. i: fundamentals and algorithms. ESA Communications, page 6.

Teunissen, P. J. and Montenbruck, O. (2017). Springer handbook of global navigation satellite systems, volume 10. Springer.

Wübbena, G. (1985). Software developments for geodetic positioning with gps using ti-4100 code and carrier measurements. In Proceedings of the first international symposium on precise positioning with the global positioning system, volume 19, pages 403–412. US Department of Commerce Rockville, Maryland.

Zhao, L., Blunt, P., and Yang, L. (2022). Performance analysis of zero-difference gps l1/l2/l5 and galileo e1/e5a/e5b/e6 point positioning using cnes uncombined bias products. Remote Sensing, 14(3):650.